Contrib Mineral Petrol (1982) 79:13–27

Contributions to Mineralogy and Petrology

Pre-Eruption History of Phyric Basalts from DSDP Legs 45 and 46: Evidence from Morphology and Zoning Patterns in Plagioclase

Lung-Chuan Kuo and R. James Kirkpatrick
Department of Geology, University of Illinois, Urbana, Illinois 61801, USA

Abstract. Phyric basalts recovered from DSDP Legs 45 and 46 contain abundant plagioclase phenocrysts which occur as either discrete single grains (megacrysts) or aggregates (glomerocrysts) and which are too abundant and too anorthitic to have crystallized from a liquid with the observed bulk rock composition. Almost all the plagioclase crystals are complexly zoned. In most cases two abrupt and relatively large compositional changes associated with continuous internal morphologic boundaries divide the plagioclase crystals into three parts: core, mantle and rim. The cores exhibit two major types of morphology: tabular, with a euhedral to slightly rounded outline; or a skeletal inner core wrapped by a slightly rounded homogeneous outer core. The mantle region is characterized by a zoning pattern composed of one to several spikes/plateaus superimposed on a gently zoned base line, with one large plateau always at the outside of the mantle, and by, in most cases, a rounded internal morphology. The inner rim is typically oscillatory zoned. The width of the outer rim can be correlated with the position of the individual crystal in the basalt pillow. The presence of a skeletal inner core and the concentration of glass inclusions in low-An zones in the mantle region suggest that the liquid in which these parts of the crystals were growing was undercooled some amount. The resorption features at the outer margins of low-An zones indicate superheating of the liquid with respect to the crystal.

It is proposed that the plagioclase cores formed during injection of primitive magma into a previously existing magma chamber, that the mantle formed during mixing of a partially mixed magma and the remaining magma already in the chamber, and that the inner rim formed when the mixed magma was in a sheeted dike system. The large plateau at the outside of the mantle may have formed during the injection of the next batch of primitive magma into the main chamber, which may trigger an eruption. This model is consistent with fluid dynamic calculations and geochemically based magma mixing models, and is suggested to be the major mechanism for generating the disequilibrium conditions in the magma.

Introduction

Extensive study of mid-ocean ridge basalt (MORB) chemistry has revealed significant local and regional variations, prompting a diversity of models for its mode of formation (e.g., Frey et al. 1974; Blanchard et al. 1976; Melson et al. 1976; Rhodes et al. 1976; Bryan and Moore 1977; White and Schilling 1978; Sun et al. 1979). It has been demonstrated that the compositional variation in MORB suites cannot, in many cases, be interpreted in terms of fractional crystallization from a single magma source. Models involving mixing of magma in chambers beneath the mid-ocean ridges appear to explain many anomalies in MORB petrology (Dungan and Rhodes 1978; Rhodes et al. 1979a, b; Walker et al. 1979).

Detailed investigations of ophiolites (e.g., Greenbaum 1972; Jackson et al. 1975; Dewey and Kidd 1977; Stern 1979; Smewing 1979; Pallister and Hopson 1981) lead to models which invoke an essentially steady-state magma chamber beneath the ridge, with new batches of primitive magma periodically injected into the chamber and mixed with the fractionated liquid in it. Normal crystal-liquid fractionation then continues until another new batch of primitive magma is injected. The geochemical consequences of this open system fractionation, as predicted by O'Hara (1977) and Pankhurst (1977), are in good agreement with chemical data from many MORB suites, implying that processes involving both fractionation and mixing may be responsible for MORB evolution.

The purpose of this paper is to examine the pre-eruption history of phyric basalts recovered from DSDP Legs 45 and 46 by studying the morphologies and zoning patterns of plagioclase crystals in these basalts. This is possible because plagioclase crystals record the physical-chemical history of magma bodies in their zoning patterns (e.g., Wiebe 1968; Pringle et al. 1974; Maaløe 1976; Uebel 1978), and because the morphologies of plagioclase crystals depend on the cooling history of the melt from which they crystallized (Lofgren 1974; Kirkpatrick et al. 1979).

Our most important conclusions are that crystallization kinetics and fluid dynamic behavior are important in controlling plagioclase crystallization and, therefore, the evolution of the magma, and that the zoning patterns and morphologies of the plagioclase phenocrysts can be explained by a model involving mixing of primitive and evolved magmas in a sub-ridge magma chamber.

General Petrography of the Phyric Basalts

The phyric basalts from Sites 395 and 396 are characterized by the presence of 20–30% plagioclase, olivine, and sometimes augitic clinopyroxene (Site 395 only) phenocrysts in a matrix of normal basalt mineralogy and texture (Natland 1979; Dungan et al. 1979b). Plagioclase is by far the most abundant. It occurs as either discrete single crystals (megacrysts) or in aggregates (glomerocrysts). We will use these terms to correspond to the terminology of Dungan and Rhodes (1978). These megacrysts

0010-7999/82/0079/0013/$03.00

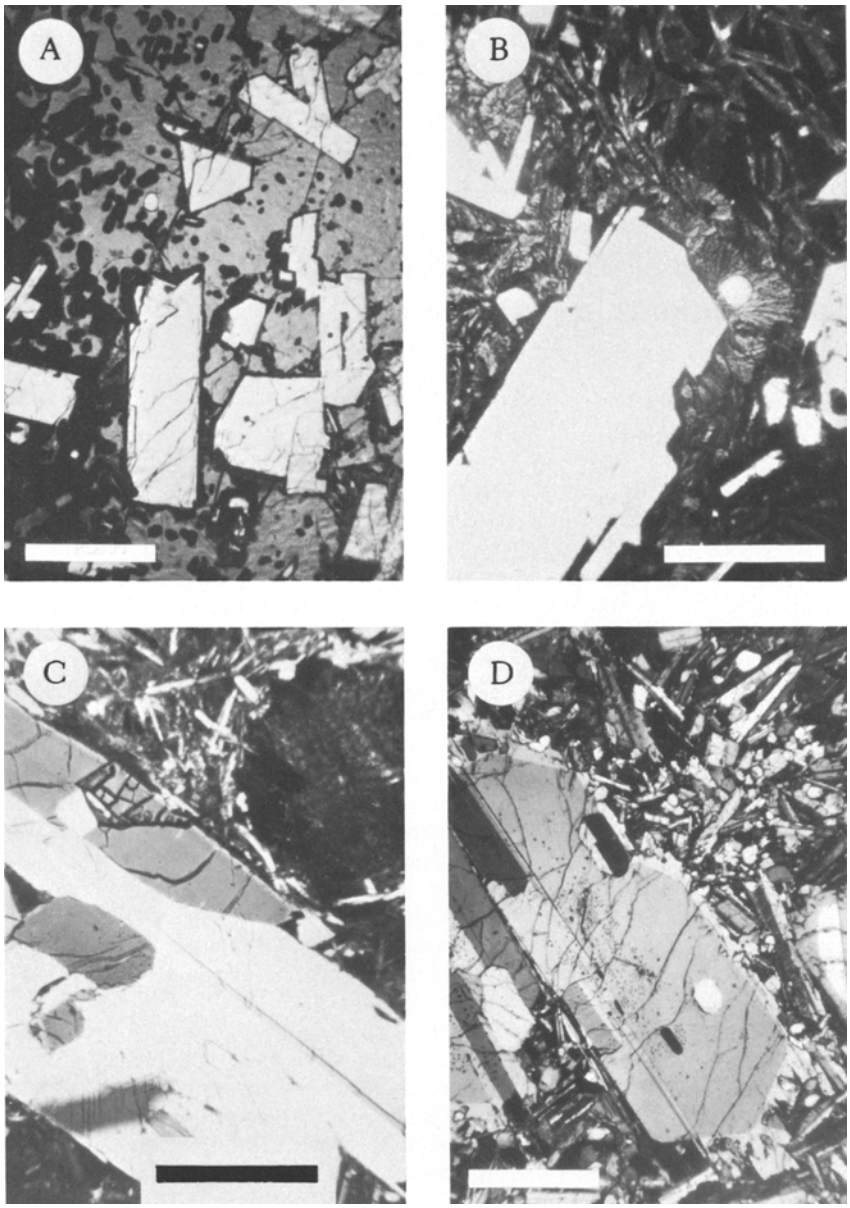

Fig. 1A–D. Photomicrographs of the external morphology of plagioclase megacrysts and glomerocrysts.
A 396B-17-3,56-60. Plagioclase megacrysts and glomerocrysts in a matrix of light brown glass and dark brown plagioclase spherulites and olivine dendrites. Thin layers of spherulitic growth have been developed around the plagioclase megacrysts and glomerocrysts. Plane polarized light. Scale bar = 1 mm.
B 395A-16-1,143-147. Plumose spherulites growing from a (001) end of a plagioclase glomerocryst and some fan spherulites from a (001) end of a small plagioclase crystal. Plane polarized light. Scale bar = 0.5 mm.
C 396-14-6,20-24. Plagioclase glomerocryst showing a curved outline due to resorption. A thin zone of post eruption growth, about 19 microns wide, occurs on the upper part of the crystal. Cross polars. Scale bar = 0.5 mm.
D 395-15-5,16-19. Part of a plagioclase glomerocryst. The euhedral plagioclase core is surrounded by a broad rim with abundant, small olivine and clinopyroxene grains included in or attached to it. The outer margin of the rim has been strongly resorbed. Crossed polars. Scale bar = 1 mm

and glomerocrysts range in long dimension from about 1 to 6 mm and are characterized by complex zoning patterns and internal morphologies and glass inclusions (many now devitrified). The glomerocrysts are composed of plagioclase grains of different size, shape, and orientation that are mutually attached in complex ways.

Morphology of Plagioclase Megacrysts and Glomerocrysts

Two categories of morphological features can be recognized in these plagioclase megacrysts and glomerocrysts; external and internal. The external morphology refers to the shapes of the outlines of these crystals. In the glassy pillow margins these outlines are perfectly preserved with no visible overgrowth (Fig. 1A). Further into a pillow, dendrite arms or fan and plumose spherulites grow from the (001) ends of the crystals (see also Plate 1 in Lofgren 1974), and there is an outer rim usually of the order of 10 microns thick in the [001] direction and thinner in the [100] or [010] directions (Fig. 1B). Even further into the pillow the outer rim width increases and the outlines of the crystals become irregular (Fig. 1C). In the pillow centers the outline of these crystals is very irregular (Fig. 1D), and the width of the outer rim reaches a maximum of about 80 microns.

The internal morphology of the crystals is defined by changes in plagioclase composition, which cause visible changes in extinction angle. There are three kinds of internal morphologies: (1) euhedral, with the compositional zones having crystallographically controlled planar boundaries; (2) skeletal, with the compositional zones having an irregular boundary with reentrants; and (3) resorbed, with curved boundaries that cross compositional zones.

Thin section observation of these crystals shows that in most cases there are two abrupt and relatively large compositional changes that coincide with continuous internal morphologic boundaries. One of them is in the central part of the crystal, whereas the other is invariably very close to the margin. These two boundaries divide the whole crystal into three parts, which

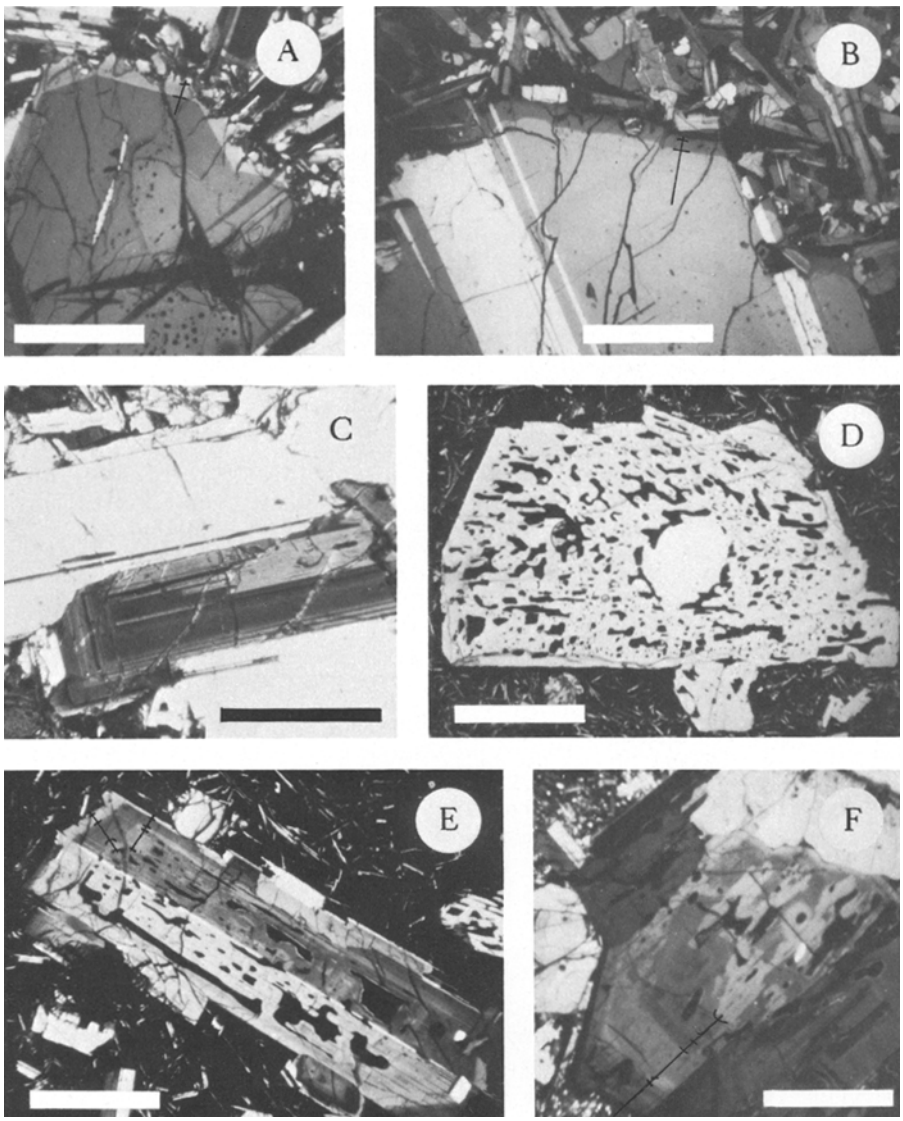

Fig. 2A–F. Photomicrographs of the internal morphology of plagioclase megacrysts and glomerocrysts. All photos were taken with crossed polars. Scale bar: 0.5 mm for (C); 1 mm for others. Lines are microprobe traverses. Cross-lines are internal morphological boundaries. **A** 395A-15-5,16-19. A simply zoned plagioclase megacryst with a euhedral core and an oscillatory zoned rim. Few inclusions are scattered in the core. **B** 395A-15-3,120-126. Part of a simply zoned glomerocryst with a homogenous core and a partly resorbed core-rim boundary. A very few inclusions are scattered in the core. **C** 395A-61-2,49-53. Part of a complexly zoned glomerocryst. All the zoning boundaries are euhedral and the whole crystal is inclusion-free. **D** 396B-20-1. Resorbed homogenous core with skeletal mantle enclosed by inclusion-free rim. The inclusions concentrated in the mantle are the liquid trapped by skeletal arms. **E** 396B-16-2,42-46. A complexly zoned glomerocryst with a skeletal core with trapped liquid inclusions. The core is enclosed by a euhedral, normal and reverse zoned mantle. **F** 395A-17-1,106-112A. A complexly zoned glomerocryst with a core consisting of a skeletal inner core and resorbed, more anorthitic outer core. The core is followed by a mantle that has skeletal and rounded morphologies. Abundant inclusions are concentrated in the narrow, more albitic zone

will be called, from inside out, core, mantle, and rim. In a few crystals the compositional difference across the core-mantle boundary is not large.

There are two types of megacryst and glomerocryst cores: type 1, those that are only slightly zoned and have a euhedral to slightly resorbed outline; and type 2, those that have a skeletal or extensively resorbed inner core which is embedded in a compositionally homogeneous, slightly rounded outer core.

Crystals with a type 1 core may or may not have a mantle (Fig. 2A, B, and C, D, respectively). Those without a mantle invariably have a large and tabular core. Crystals with type 2 cores always have a well developed mantle. These skeletal cores are very similar to those described by Maaløe (1976) from the Upper Zone of the Skaergaard intrusion, Greenland.

Because of the complex combinations of euhedral and skeletal morphologies and various degrees of resorption, morphologic variations in the mantle of these crystals are much more complicated than in the cores. For instance, the mantle may exhibit repeated euhedral zones (Fig. 2C), skeletal morphology only (Fig. 2D), repeated resorption (Fig. 2E), or a combination of skeletal morphology and resorption (Fig. 2F). All these variations are associated with compositional changes. The term complexly zoned plagioclase will be applied to these crystals with complex mantles. It appears that the occurrence of complexly zoned plagioclase is one of the outstanding petrographic features of mid-Atlantic ridge basalts (e.g., Muir and Tilley 1964; Blanchard et al. 1976; Bryan and Moore 1977; Shibata et al. 1979; Natland 1979) and also of some oceanic island basalts (e.g., Imsland et al. 1977).

In summary, the plagioclase megacrysts and glomerocrysts in these rocks can be divided into two categories: simply zoned and complexly zoned. The simply zoned crystals are characterized by the absence of a mantle and the presence of a euhedral, slightly zoned tabular core. Complexly zoned plagioclases are characterized by a complex mantle region. Of these there are two sub-types: those with a euhedral to resorbed, compositionally homogeneous core, and those with a skeletal or strongly resorbed inner core enclosed by a rather homogeneous outer core.

The mantle regions typically show complex internal morphological variations associated with abrupt compositional changes.

Both major types have an inner rim region around the whole crystal with a prominent compositional hiatus across the mantle-rim or core-rim boundary. The thickness of the inner rims of the Site 395 plagioclase generally is 40–120 microns in [001], while those of the Site 396 plagioclase are narrower-about 30–70 microns. Both types also have a ragged outer rim if they are in pillow interiors but not if they are near pillow margins.

These morphologic variations, together with the fact that the composition of the outer rim is the same as that of the groundmass plagioclase, indicate that the external morphology of these crystals is controlled by the post-eruption cooling rate. The internal morphologic and compositional variations are not related to position of the crystal in the pillows and, therefore, reflect the pre-eruption history of the magma.

Plagioclase Compositions

Analytical Methods

Quantitative analyses from 31 plagioclase megacrysts and glomerocrysts have been obtained by electron microprobe analysis. The locations of the profiles were chosen by the following criteria: (1) they pass along the direction in the crystal in which the most complete zoning history in that part of the crystal is recorded, (2) they avoid cracks and inclusions so that every zone in the profile occurs in the microprobe traverse, and (3) they are as parallel as possible to crystallographic axes so that intergranular comparisons can be reasonably made. In most cases 1 to 4 profiles in each megacryst and 3 to 8 profiles in each glomerocryst were run.

Reconnaissance traverses of selected plagioclase crystals were made for Ca using an ARL-EMX electron microprobe with a beam current of approximately 0.1 microamps and a scan speed of 96 microns/minute. The different varieties of zoning patterns were recognized from these. Representative profiles of each type have been duplicated using a JEOL JXA-50A electron probe microanalyzer with a sample current of approximately 0.035 microamps (about 4,000–7,000 cps for Ca) and a scan speed of 20 microns/minute. The excellent reproducibility of detailed zoning patterns indicates that a microprobe traverse is a reliable means of investigating continuous chemical variations along a compositionally heterogeneous profile (Subbarao et al. 1972).

Quantitative analyses were carried out on the ARL-EMX electron microprobe using a beam current of approximately 0.08 microamps for Ca, Si, Na and 0.2 microamps for Fe, Al, Mg, an accelerating voltage of 20 kV, and a beam diameter of 1 micron. The standard used was labradorite from Lake County, Oregon (Stewart et al. 1966, Table 1). Drift, background and dead time corrections were made using the program PROBE, and absorption, fluorescence, backscatter, and stopping power corrections with a modified version of ABFAN (Boyd et al. 1969). Three to 8 point analyses were made along each traverse to calibrate the qualitative zoning profiles. The accuracy of the calibration is about 1.4% relative at the 95.4% confidence level. Representative analyses are presented in Tables 1 and 2.

Simply Zoned Plagioclase

The cores of this kind of plagioclase are typically tabular and slightly oscillatory zoned in the range 84–88% An. The amplitude of the oscillatory zoning is about 1–4% An. The compositions

Table 1. Representative electron microprobe analyses of simply zoned plagioclases. (Points correlated to Fig. 3)

	395A-15-5,16-19 (a)*			395A-17-1,106-112B (a)			
	1	2	3	1	2	3	4
SiO_2	45.53	50.64	51.10	46.28	45.35	50.01	50.60
Al_2O_3	34.26	30.32	30.54	34.35	34.39	31.96	31.20
MgO	0.31	0.55	0.30	0.36	0.36	0.49	0.45
FeO	0.33	0.57	0.67	0.36	0.40	0.45	0.45
CaO	17.66	13.50	13.95	17.37	17.72	15.01	14.78
Na_2O	1.54	3.47	3.54	1.36	1.15	2.61	2.86
Total	99.63	99.05	100.10	100.08	99.37	100.53	100.34
An	86.5	68.3	68.6	87.6	89.5	76.1	74.0
Ab	13.5	31.6	31.4	12.4	10.5	23.9	26.0
Si	2.108	2.327	2.328	2.127	2.104	2.270	2.300
Al	1.869	1.644	1.641	1.860	1.880	1.710	1.671
Mg	0.021	0.038	0.020	0.025	0.025	0.033	0.030
Fe	0.013	0.022	0.025	0.014	0.015	0.017	0.017
Ca	0.876	0.665	0.681	0.855	0.880	0.730	0.720
Na	0.138	0.310	0.313	0.121	0.103	0.229	0.252
Total	5.025	5.006	5.008	5.002	5.007	4.989	4.990

* Alphabets indicate crystals in the same sample

are the same as those calculated by Rhodes et al. (1979b) from their estimated primitive magma composition. The cores are either homogeneous (Fig. 3A) or can be compositionally subdivided into inner and outer cores. In the latter case the outer core has a slightly higher An content than the inner core and is very gently normally zoned (Fig. 3B).

The rims can be divided into inner and outer rims. The inner rims are characterized by several 10–15 micron wide oscillatory zones superimposed on gentle normal zoning. The composition is in the range 65–78% An, depending on the composition of the chemical unit the host rock belongs to. The amplitude of this oscillatory zoning is no more than 2–5% An. The outer rims contain about 5% An less than the inner rims.

Complexly Zoned Plagioclase

At least 80% of the plagioclase megacrysts and glomerocrysts are complexly zoned. Core compositions of these crystals vary from 75 to 88% An and are related to core morphology. High-An cores are similar to the cores of the simply zoned plagioclase (e.g., Fig. 4D, H). More often, however, the cores of the complexly zoned plagioclases are skeletal and less anorthitic (e.g., Fig. 4A, B, F, G). In a few cases, a strongly resorbed inner core (75–82% An) is enclosed in a more anorthitic, slightly oscillatory zoned outer core (Fig. 4E). In these crystals the composition of the mantle immediately adjacent to the core is always in the range 82–77% An. Consequently, a high-An, tabular core is usually surrounded by a compositional hiatus, while a low-An, skeletal core is frequently surrounded by a region of reverse zoning.

Details of the zoning patterns in the mantle regions vary considerably, but two significant features occur in almost all of them: several spikes or plateaus of high An content, and a very limited range in composition of the base line on which these spikes/plateaus are superimposed. The composition of each spike or plateau is 3–7% An higher than that of the segments

of base line next to it. Some sharp and narrow spikes do not appear on all traverses through a single crystal (e.g., Fig. 4F and G). Most plateaus can be correlated from traverse to traverse in a given crystal. These are reversely zoned, with a 2 to 6% increase in An from inside to outside. There are 1 to 3 plateaus in each complexly zoned plagioclase, with one of them always occupying the outermost part of the mantle. This outer plateau usually has the highest An content of any plateau in the mantle, in many cases as high as that of the euhedral cores (84–88% An). For zoning profiles with several spikes and plateaus, the compositional difference between the spikes/plateaus and the base line decreases outwards, and there is no significant intergranular correlation in the position of these spikes and plateaus before the last plateau.

The base line composition in the mantle is usually in the range 74.5–79.5% An. The one exception is a plagioclase in sample 395A-16-1,143-147, in which the range is 86–83% An. The highest base line An content is in the innermost mantle, with the value dropping slowly to a minimum value in the central part of the mantle. From this point the base line composition may be constant, may show gentle reverse zoning, or may be constant and then show reverse zoning. In all cases the reverse zone is very narrow.

The rim of the complexly zoned plagioclases always surrounds the entire crystal, with a decrease of 6–13% An across the mantle-rim boundary. In general the rim profile is composed of a wide plateau (inner rim) followed by a thin layer with steep normal zoning (outer rim). The inner rim shows various

Table 2. Representative electron microprobe analyses of complexly zoned plagioclases. (Points correlated to Fig. 4)

	395A-30-1,73-78 (a)											
	1	2	3	4	5	6	7	1	2	3	4	5
SiO_2	48.89	50.10	47.20	49.39	50.54	48.55	51.23	49.74	49.06	49.88	47.83	48.05
Al_2O_3	31.17	30.81	32.05	32.27	30.78	32.08	30.54	31.36	31.86	30.82	32.60	32.09
MgO	0.48	0.41	0.35	0.30	0.35	0.28	0.43	0.41	0.38	0.36	0.26	0.33
FeO	0.51	0.49	0.48	0.50	0.48	0.51	0.50	0.51	0.50	0.51	0.48	0.50
CaO	15.40	15.23	16.64	15.60	15.07	16.42	14.30	16.14	15.94	15.18	16.89	16.41
Na_2O	2.81	2.81	2.05	2.50	2.87	2.10	3.33	2.38	2.23	2.81	1.88	2.24
Total	99.26	99.85	98.77	100.56	100.09	99.94	100.33	100.54	99.97	99.56	99.94	99.62
An	75.1	74.9	81.8	77.4	74.5	81.2	70.4	74.9	79.8	74.9	83.1	80.3
Ab	24.9	25.1	18.2	22.6	25.5	18.8	29.6	25.1	20.2	25.1	16.9	19.7
Si	2.257	2.294	2.198	2.248	2.306	2.229	2.328	2.267	2.247	2.291	2.200	2.216
Al	1.697	1.662	1.759	1.730	1.655	1.735	1.636	1.684	1.719	1.668	1.766	1.744
Mg	0.033	0.028	0.024	0.020	0.024	0.019	0.029	0.028	0.026	0.025	0.018	0.023
Fe	0.020	0.019	0.019	0.019	0.018	0.020	0.019	0.020	0.019	0.020	0.018	0.019
Ca	0.762	0.747	0.830	0.760	0.737	0.807	0.696	0.788	0.782	0.747	0.831	0.811
Na	0.252	0.249	0.185	0.221	0.254	0.187	0.293	0.210	0.198	0.250	0.168	0.200
Total	5.021	4.999	5.015	4.998	4.994	4.997	5.001	4.997	4.991	5.001	5.001	5.013

	395A-17-1,126-128 (a)			396-14-6,20-24 (b)							
	1	2	3	1	2	3	4	1	2	3	4
SiO_2	48.33	49.13	46.49	46.67	49.87	48.62	50.91	47.06	49.06	49.67	50.53
Al_2O_3	32.99	32.20	33.03	33.51	32.04	31.95	31.56	33.38	32.46	31.08	30.61
MgO	0.41	0.41	0.38	0.33	0.44	0.44	0.49	0.16	0.28	0.30	0.38
FeO	0.48	0.48	0.46	0.39	0.45	0.45	0.59	0.42	0.44	0.42	0.53
CaO	16.48	16.30	17.93	17.43	15.67	15.91	14.50	17.42	15.80	15.24	14.72
Na_2O	2.08	2.02	1.43	1.42	2.18	2.16	2.79	1.49	2.33	2.71	3.06
Total	100.77	100.54	99.72	99.75	100.65	99.53	100.84	99.93	100.37	99.42	99.83
An	81.4	81.7	87.4	87.1	79.9	80.2	74.2	86.6	79.0	75.8	72.6
Ab	18.6	18.3	12.6	12.9	20.1	19.8	25.8	13.4	21.0	24.2	27.4
Si	2.202	2.239	2.152	2.153	2.263	2.237	2.300	2.166	2.237	2.283	2.311
Al	1.770	1.728	1.800	1.821	1.713	1.732	1.680	1.810	1.744	1.683	1.650
Mg	0.028	0.028	0.026	0.023	0.030	0.030	0.033	0.011	0.019	0.020	0.026
Fe	0.018	0.018	0.018	0.015	0.017	0.017	0.022	0.016	0.017	0.016	0.020
Ca	0.804	0.795	0.888	0.862	0.761	0.784	0.702	0.859	0.771	0.751	0.722
Na	0.183	0.179	0.128	0.127	0.192	0.193	0.244	0.133	0.206	0.242	0.271
Total	5.005	4.987	5.012	5.001	4.976	4.993	4.981	4.995	4.994	4.995	5.000

Table 2 (continued)

	395A-33-2,52-56 (d)									
	1	2	3	4	5	1	2	3	4	5
SiO_2	48.69	48.65	48.03	48.77	48.05	49.91	48.09	47.93	46.91	49.74
Al_2O_3	31.74	32.90	32.72	31.68	32.70	31.11	32.39	33.10	33.19	30.72
MgO	0.38	0.38	0.38	0.43	0.43	0.46	0.39	0.44	0.43	0.41
FeO	0.39	0.35	0.39	0.39	0.39	0.41	0.36	0.37	0.37	0.49
CaO	16.21	16.35	16.68	16.00	16.88	15.08	16.22	16.41	16.91	14.76
Na_2O	1.92	1.97	1.90	2.36	1.68	2.74	2.12	2.02	1.73	2.89
Total	99.33	100.60	100.10	99.63	100.13	99.71	99.57	100.27	99.54	99.01
An	82.3	82.0	83.0	78.9	84.8	75.4	81.0	81.8	84.4	73.9
Ab	17.7	18.0	17.0	21.1	15.2	24.6	19.0	18.2	15.6	26.1
Si	2.245	2.215	2.203	2.243	2.202	2.286	2.214	2.192	2.166	2.294
Al	1.723	1.765	1.767	1.717	1.766	1.679	1.757	1.784	1.806	1.670
Mg	0.026	0.026	0.026	0.029	0.029	0.032	0.027	0.030	0.029	0.028
Fe	0.015	0.013	0.015	0.015	0.015	0.016	0.014	0.014	0.014	0.019
Ca	0.800	0.797	0.819	0.789	0.829	0.740	0.800	0.804	0.837	0.730
Na	0.172	0.173	0.169	0.211	0.149	0.243	0.189	0.179	0.155	0.259
Total	4.981	4.989	4.999	5.004	4.990	4.996	4.991	5.003	5.007	5.000

	396B-22-2,3-6 (c)			395A-16-1,143-147 (a)				
	1	2	3	1	2	3	4	5
SiO_2	46.82	49.40	47.97	45.97	46.08	46.50	45.85	49.62
Al_2O_3	33.36	32.41	31.65	33.98	34.39	33.66	33.84	31.38
MgO	0.28	0.35	0.33	0.44	0.36	0.43	0.34	0.43
FeO	0.39	0.42	0.46	0.33	0.37	0.37	0.33	0.51
CaO	16.63	15.38	16.67	17.24	17.89	16.91	17.65	15.23
Na_2O	1.83	2.51	2.04	1.51	1.20	1.84	1.37	2.75
Total	99.31	100.47	99.12	99.47	100.29	99.71	99.38	99.92
An	83.4	77.2	82.0	86.2	89.1	83.7	87.7	75.3
Ab	16.6	22.8	18.0	13.8	10.9	16.3	12.3	24.7
Si	2.166	2.248	2.224	2.127	2.117	2.146	2.126	2.271
Al	1.819	1.737	1.728	1.853	1.862	1.831	1.849	1.693
Mg	0.019	0.023	0.023	0.031	0.025	0.029	0.024	0.029
Fe	0.015	0.016	0.018	0.013	0.014	0.014	0.013	0.020
Ca	0.824	0.749	0.828	0.855	0.881	0.836	0.877	0.747
Na	0.164	0.222	0.183	0.136	0.107	0.164	0.123	0.244
Total	5.007	4.995	5.004	5.015	5.006	5.020	5.012	5.004

combinations of normal, reverse and constant composition zoning patterns and a range of compositions of 78–68% An. The inner rim is typically oscillatory zoned. Each oscillation is less than 1% An and is too narrow to be resolved by the microprobe. The outer rim composition is less than about 70% An and is identical to the groundmass plagioclase composition (Dungan et al. 1979a, b; Kirkpatrick 1979a).

Iron and Magnesium in Plagioclase

Figures 5 and 6 show the relationships between the major element compositions of the plagioclases (% An) and Mg/(Mg+Fe) values for the core and inner rim of Site 395 plagioclases. The positive correlation between Mg/(Mg+Fe) and An content in both simply and complexly zoned plagioclase cores is identical no matter which chemical unit these crystals come from. The same positive correlation is shown in the inner rim (Fig. 6), but the Mg/(Mg+Fe) values of plagioclases from chemical units P3, P4 and P5 have about the same range and are higher than those from unit P2. The whole rock Mg/(Mg+Fe) ratios show the same variation among chemical units (Rhodes et al. 1979a). It appears, then, that the core compositions do not reflect the present composition of the host basalt, whereas the inner rim composition does.

Glass Inclusions

Both the olivine and plagioclase phenocrysts contain various numbers of glass inclusions. Inclusions in olivine usually number 1 to 3 per grain, and have spherical or subspherical shapes (Dun-

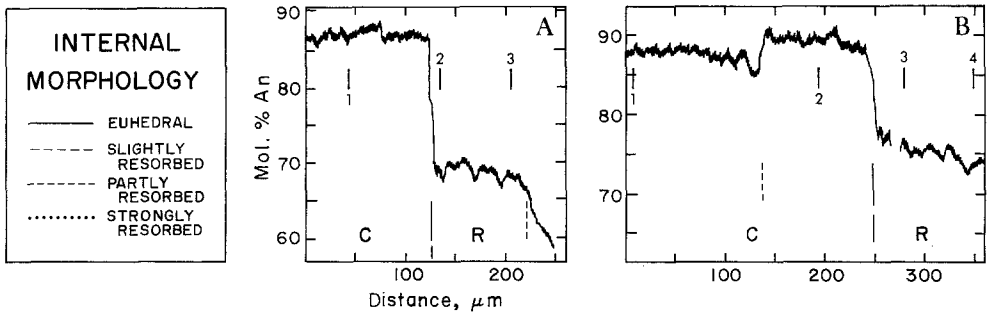

Fig. 3A, B. Zoning pattern in simply zoned plagioclase. **A** 395A-15-5,16-19. A traverse parallel to [001] showing an essentially homogenous core of An_{87}. **B** 395A-17-1,106-112. A traverse parallel to [001]. The core is divided into two parts by a slightly resorbed boundary. The vertical bars with a number indicate the position of microprobe analysis used to calibrate the zoning profile. The unnumbered vertical bars divide the core (*C*) and rim (*R*). Patterned bars indicate the observed internal morphology of the crystal (see the legend at *left*)

gan and Rhodes 1978). In plagioclase the number of inclusions varies from almost none to hundreds per grain. The glass inclusions in plagioclase can be divided into two categories based on their shape, size, distribution and origin.

Inclusions of the first type vary in shape from spherical to subspherical to subangular and have diameters ranging from 2 to 40 microns. The inclusion material is glassy in small inclusions but devitrified to a dark-brown color in large ones (Fig. 7A–D). Only a few inclusions contain spherical vapor bubbles, indicating a very low volatile content in the host magma (Delaney et al. 1977; see Watson 1976, for a contrary case). This type of inclusion occurs as scattered individuals in the large, tabular, slightly zoned crystals (Fig. 7A), in arrays or clusters that are concentrated in zones or patches more albitic than the surrounding parts of the crystal, or between segments of skeletal crystal (Fig. 7B, C), or both (Fig. 7D). Some of these inclusions occur along twin planes. In many cases there is a thin layer of more albitic plagioclase surrounding the inclusion, indicating growth into the inclusion after it formed.

Glass inclusions of the second type (Figs. 7E–F) have an irregular shape and variable size, distribution, and composition depending on their mode of formation. Many of these inclusions apparently represent cross-sections through short-range tunnel systems which have axes roughly coincident with the major crystallographic axes of the host plagioclase. The longest dimensions of these tunnel systems range from about 80 microns to 1.5 mm. Despite their irregular shape, these inclusions tend to be elongated along [001] of the host crystal and are invariably dark and glassy. Continued growth of the trapped liquid is common, resulting in thin (of the order of microns), more albitic layers on the inclusion walls.

This second type of inclusion occurs in several ways. (1) In some skeletal crystals the original crystal grew at the expense of liquid trapped between skeleton arms, resulting in zoning sub-parallel to the skeletal outline. These inclusions represent the remnant liquid trapped between skeletal arms. Therefore, their distribution is related to the shape of the skeletal crystal, and their pattern generally lacks long distance alignment (Figs. 2D, E, and F; 7E). Inclusions associated with skeletal growth or resorption may also occur in certain zones in the crystal (Fig. 2D; see also Fig. 2F in Rhodes et al. 1979b). (2) Some occur in relatively homogeneous plagioclase crystals. In this case, the inclusions tend to be bounded by and aligned with polysynthetic twins (Fig. 7F, see also Dungan and Rhodes 1978). They are usually smaller and more abundant in highly twinned plagioclase but are large and blocky in the crystals with only a few composition planes. (3) Some occur along the boundaries of attached crystals in glomerocrysts. These are typically irregular in size and shape and have a scattered distribution (Fig. 8). (4) Some are aligned along the faceted boundaries of the larger plagioclases in glomerocrysts. These are more or less rectangular in shape, and their short ends are bounded by (001) faces of smaller plagioclases attached parallel to the large one.

Mutual Attachment of Plagioclase Grains

A complicated mode of attachment of individual crystals in glomerocrysts is a significant feature of the plagioclase in these basalts. In fact, the number of glomerocrysts is larger than the number of single phenocrysts in all the samples examined, indicating that mutual attachment of plagioclase crystals is a common occurrence.

A typical glomerocryst is illustrated in Fig. 8A. The first boundary, labeled 1, clearly formed shortly after the formation of the skeletal inner cores. The cores were not euhedral, but are still attached to one another along interfaces sub-parallel to (010). The second stage of attachment is marked by the attachment of an anhedral plagioclase with a skeletal core to the left side and an elongated plagioclase blade to the right side of the central glomerocryst along the boundaries labeled 2. In the light of subtle differences in zoning sequence between the upper and the left part of the interface, the latter one might have initially touched the host crystal diagonally and then rotated clockwise towards it. The former one, on the other hand, apparently stuck into a reentrant and was not able to align itself with the host crystal. The growth of the mantle on the right side of the crystal is locally disrupted by several plagioclase laths along the boundaries labeled 3. The interface, labeled 4, between the host and the attached crystals of the last stage is typically very close to the mantle-rim boundary.

Another glomerocryst is shown in Fig. 8B. This cluster is composed of two smaller glomerocrysts combined along the boundary labeled 2. The one on the left is composed of several slightly oscillatory zoned plagioclase crystals while the one on the right is a large, polysynthetically twinned crystal with a few smaller crystals around it. The boundaries between the crystals that formed these two smaller glomerocrysts are labeled 1, although the two events may not be contemporaneous. Evidence that 2 is slightly later than 1 is from the zoning sequence difference between the two planes in the grain labeled a. The third stage is again characterized by many small crystals attached parallel to the edges and in reentrants of the host plagioclase.

There are three possible processes that could cause the widespread occurrence of glomerocrysts: (1) heterogeneous nucleation, (2) accumulation, and (3) synneusis. Heterogeneous nucleation can be ruled out because of the variable zoning patterns

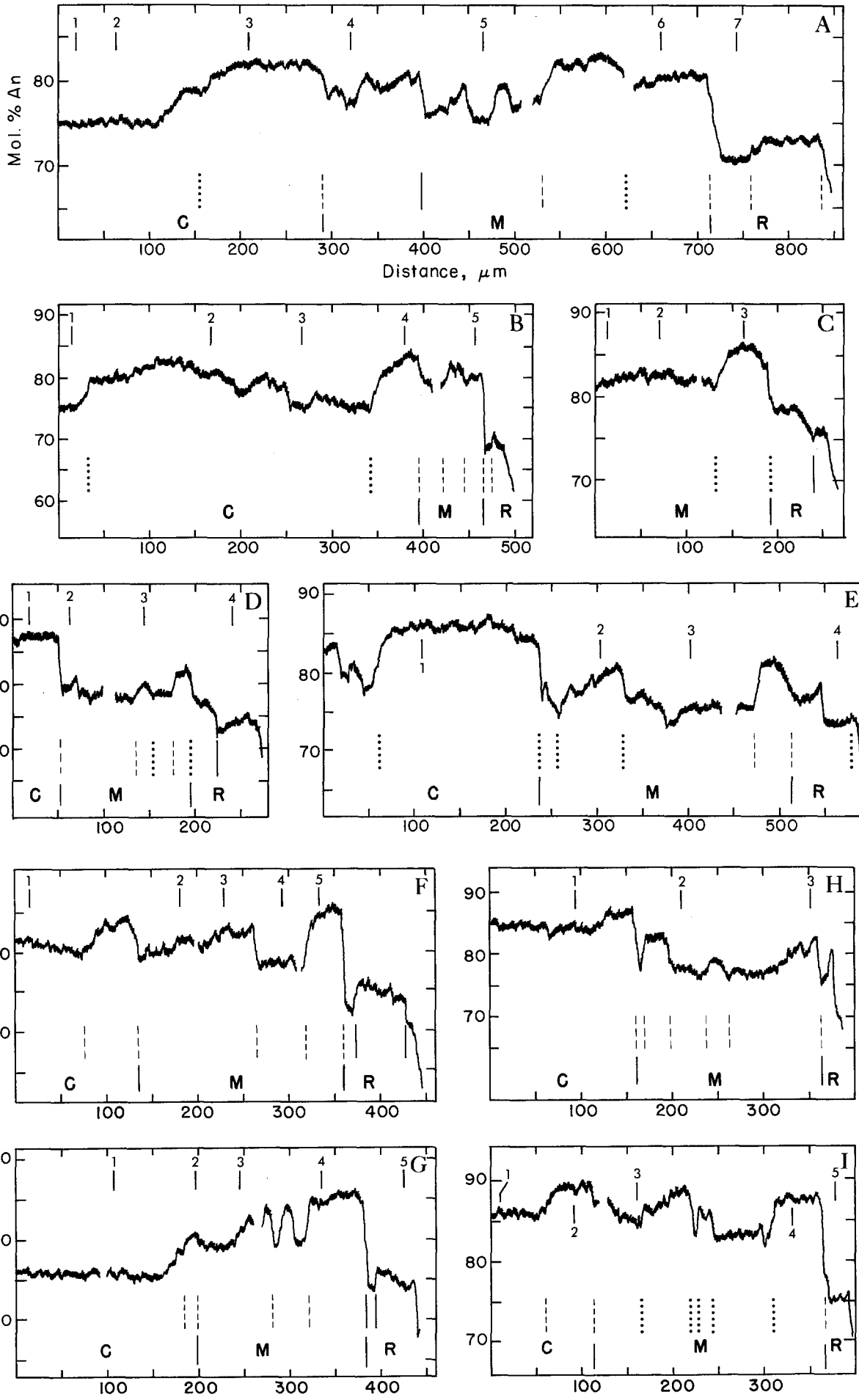
A
Mol. % An
80
70
C
M
R
100
200
300
400
500
600
700
800
Distance, μm
B
90
80
70
60
C
M
R
100
200
300
400
500
C
90
80
70
M
R
100
200
D
90
80
70
C
M
R
100
200
E
90
80
70
C
M
R
100
200
300
400
500
F
80
70
C
M
R
100
200
300
400
H
90
80
70
C
M
R
100
200
300
G
90
80
70
C
M
R
100
200
300
400
I
90
80
70
C
M
R
100
200
300

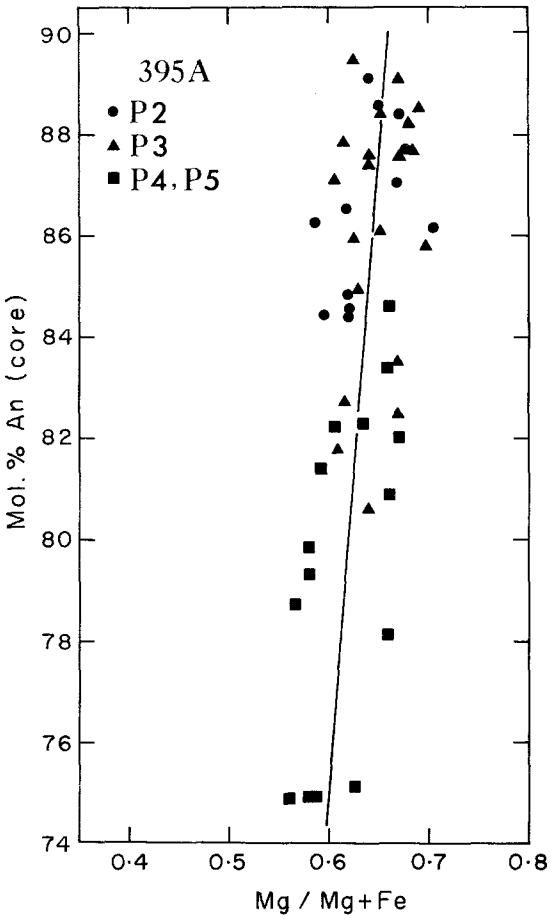

Fig. 5. Crystal composition versus Mg/(Mg+Fe) ratio for the cores of plagioclases from Site 395A phyric basalts. The slope calculated using the equations of Longhi (1976) for the temperature dependence of the distribution coefficients of Mg and Fe in plagioclase-basalt system is also shown. The position of the line is arbitrarily drawn to fit the data

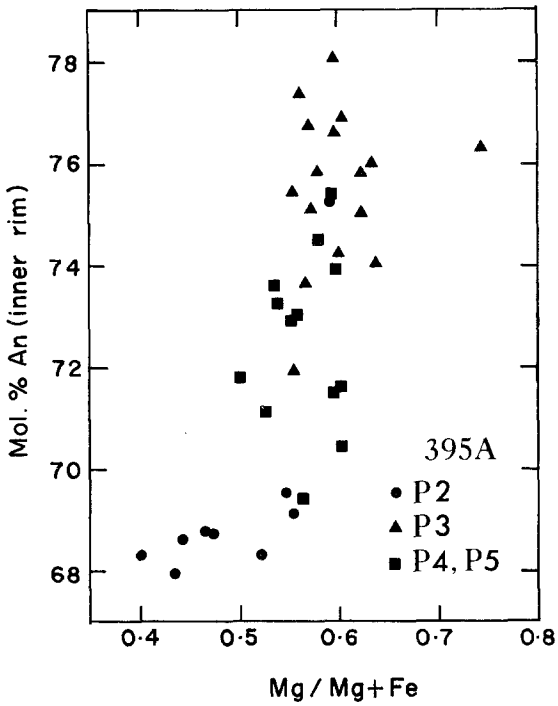

Fig. 6. Crystal composition versus Mg/(Mg+Fe) ratio of the inner rim of plagioclases from Site 395A phyric basalts

of the individual crystals in a glomerocryst. Accumulation is unlikely because (1) the attachment of plagioclase is episodic in nature, whereas a relatively continuous process of attachment is expected during accumulation, (2) if the accumulation is due to the sinking of crystals, then the major accumulated phases should be olivine, plagioclase and pyroxene or plagioclase and pyroxene (Irvine 1979). Neither are common in these rocks, (3) if accumulation occurred, then a plagioclase on the bottom of a magma body should continue to grow only on the upper side of the crystal, and therefore an asymmetric zoning pattern should be observed. This is inconsistent with our data. Therefore, it is most likely that synneusis is the major process by which the glomerocrysts formed.

Vance (1969) has defined synneusis as the process of drifting-together and mutual attachment of crystals suspended in a liquid. Plagioclase crystals in a synneusis relationship are preferentially joined along their broader (010) faces such that they appear sub-parallel. The external morphologic irregularities of the crystals in a synneusis relationship tend to be eliminated by post-synneusis growth. Crystals in a synneusis relationship can be distinguished from crystals in an epitaxial relationship because synneusis crystals are relatively large when they are initially attached, as indicated by their well-developed zoning sequences, and by the length of their contact, or their external crystal form. According to these criteria, it appears that most plagioclase glomerocrysts in these rocks exhibit a multi-stage synneusis relationship. In this context, there are several generalizations can be

Fig. 4A–I. Representative zoning patterns of complexly zoned plagioclases. Unnumbered vertical bars divide core (*C*), mantle (*M*) and rim (*R*). See Fig. 3 for patterns indicating internal morphologies. **A** and **B** 395A-30-1,73-78,a. **A** deviates slightly from [001], and **B** is parallel to [100] in the same crystal as part of a glomerocryst. The crystal has a skeletal inner core about 350 microns wide surrounded by the homogeneous outer core. The mantle is well developed at the [001] ends but is shortened and partly absent in the [100] direction. Note the appearance of several spikes and plateaus in the mantle and the gently normal zoned and then reverse zoned base line. The rim is oscillatory zoned. **C** and **D** 395A-17-1,126-128,a. **C** is parallel to [100] and **D** deviates slightly from [100] in the same megacryst. It has a skeletal inner core (An_{80}) enclosed by a homogeneous outer core of An_{87}. The mantle is composed of several small spikes superimposed on a slightly normal zoned base line and ends with a plateau region. **E** 396-14-6,20-24,b. A traverse oblique to [001] of a megacryst with a strongly resorbed inner core surrounded by a homogenous outer core. The base line in the mantle is in the range An_{75-77}. The small region of low An content at 370 to 390 microns is a local patch in the crystal. Again there are several spikes and plateaus, with one of them at the outermost part of the mantle. The rim is composed of two reverse zones with a stepwise decrease in An content between them. **F** and **G** 395A-33-2,52-56,d. Two traverses are parallel to [001] at either end of a crystal as part of a glomerocryst. The features in the core and mantle are very similar to those in **C** and **D**. The narrow spike at about 300 microns is a local feature. **H** 396B-22-2,3-6,c. A traverse is oblique to [001] of a crystal as part of a glomerocryst. The base line in the mantle is slightly normal zoned and then reversed zoned. Note the gradual decrease in size and composition of the spikes and plateaus in the mantle before the appearance of the last plateau. The rim is reverse zoned. **I** 395A-16-1,143-147,a. A traverse parallel to [001] of a crystal which is part of a glomerocryst. The inner core is skeletal and the outer core is homogeneous. The features in the mantle are similar to those in **H**

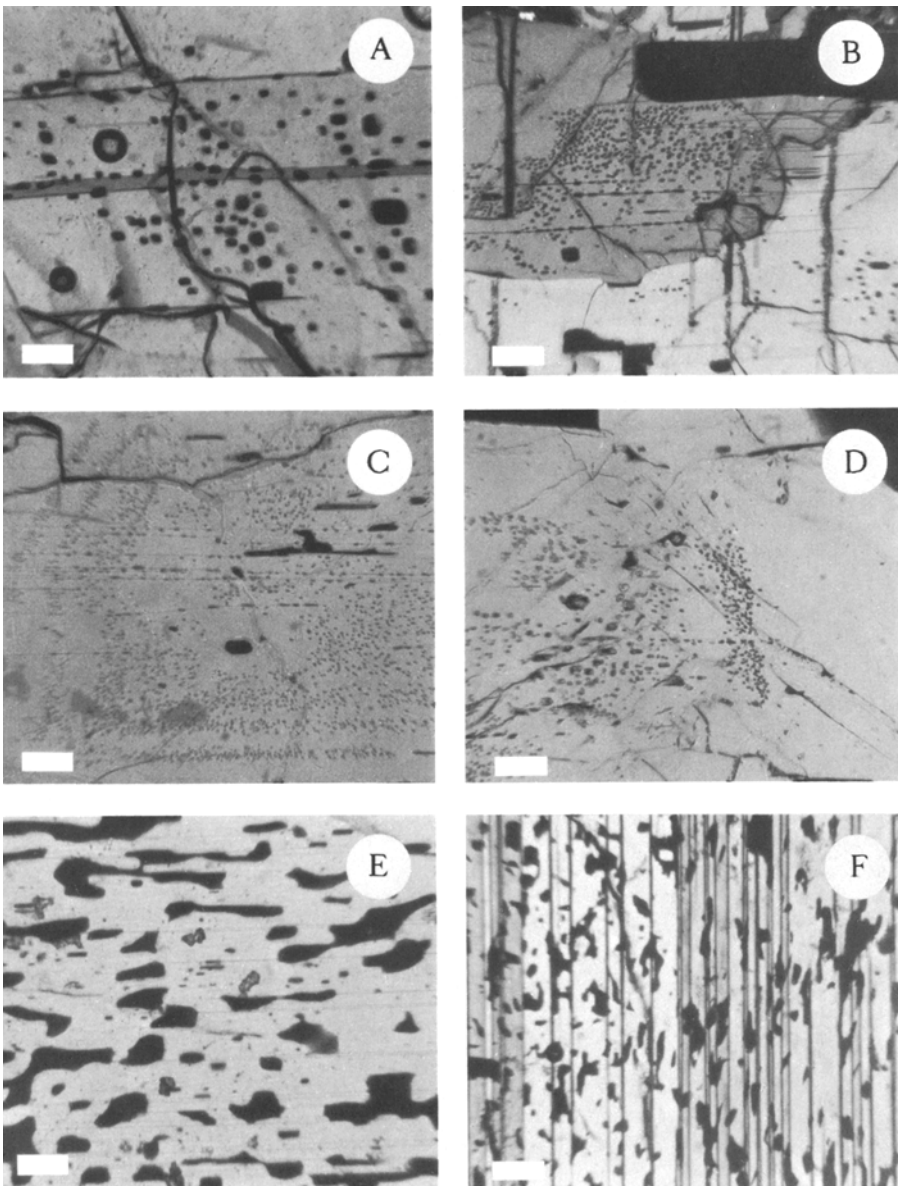

Fig. 7A–F. Photomicrographs of glass inclusions in plagioclase. **A, B, F:** crossed polars. **C, D, E:** plane light. Scale bar = 100 microns.
A 396B-17-3,56-60. Sub-angular, devitrified glass inclusions randomly distributed in a homogeneous plagioclase host.
B 395A-17-1,106-112A. Clear glass inclusions concentrated in a skeletal core more albitic than the surrounding mantle.
C 395A-17-1,106-112A. Periodic, dense arrays of spherical inclusions coincident with compositional zoning in the host megacryst.
D 395A-16-1,143-147. An array of subspherical, clear, glass inclusions within a zoned plagioclase. Inclusions in the core region are randomly distributed.
E 396B-17-3,56-60. Glass inclusions in a skeletal core.
F 396B-18-1,21-27. Grid-patterned inclusions strongly controlled by polysynthetic twin lamellae, which occur throughout the whole crystal

made about the synneusis relationship in these glomerocrysts: (1) the synneusis appears to have occurred episodically, shortly after the core formation, with the growth of the outermost part of the mantle, and during the early stage of rim development, (2) the mutual attachment of two kinds of cores, as described above, in the first episode of synneusis is very rare, (3) the last stage of synneusis is characterized by the attachment of numerous small plagioclases onto a big glomerocryst.

Discussion

Physical-chemical factors pertaining to the magma chamber which may govern the variations in plagioclase composition and morphology include temperature, pressure, undercooling, superheating, magma mixing, and convection. These are evaluated in this section.

Temperature and Pressure Effects

Variation in equilibrium plagioclase composition as a function of temperature and pressure has been discussed for the system albite-anorthite by Lindsley (1966) and Yoder (1969). The equilibrium plagioclase becomes more albitic with decreasing temperature isobarically but with increasing pressure isothermally. For instance, at a pressure of 1 atm, the plagioclase in equilibrium with a liquid composition of 65% An is about 90% An at 1,485° C. At 10 kb pressure (dry) and 1,485° C, the liquid of 65% An is supercooled by about 70° C and the equilibrium plagioclase is 80% An and the equilibrium liquid is 46% An.

For basaltic compositions the effect of pressure on the equilibrium plagioclase composition is the same as for the system albite-anorthite (Green 1967). Variation of the plagioclase composition with water pressure is not important because of the very low water content (less than 0.01% wt. water) in the MORB (Delaney et al. 1977).

Smith (1975) has suggested that the Fe and Mg contents of plagioclase depend largely on the temperature of crystallization and composition of the host magma. Longhi (1976) studied the distribution coefficients of Mg and Fe in the natural plagioclase-basalt systems and concluded that Mg in plagioclase increases slightly with decreasing temperature. He also inferred

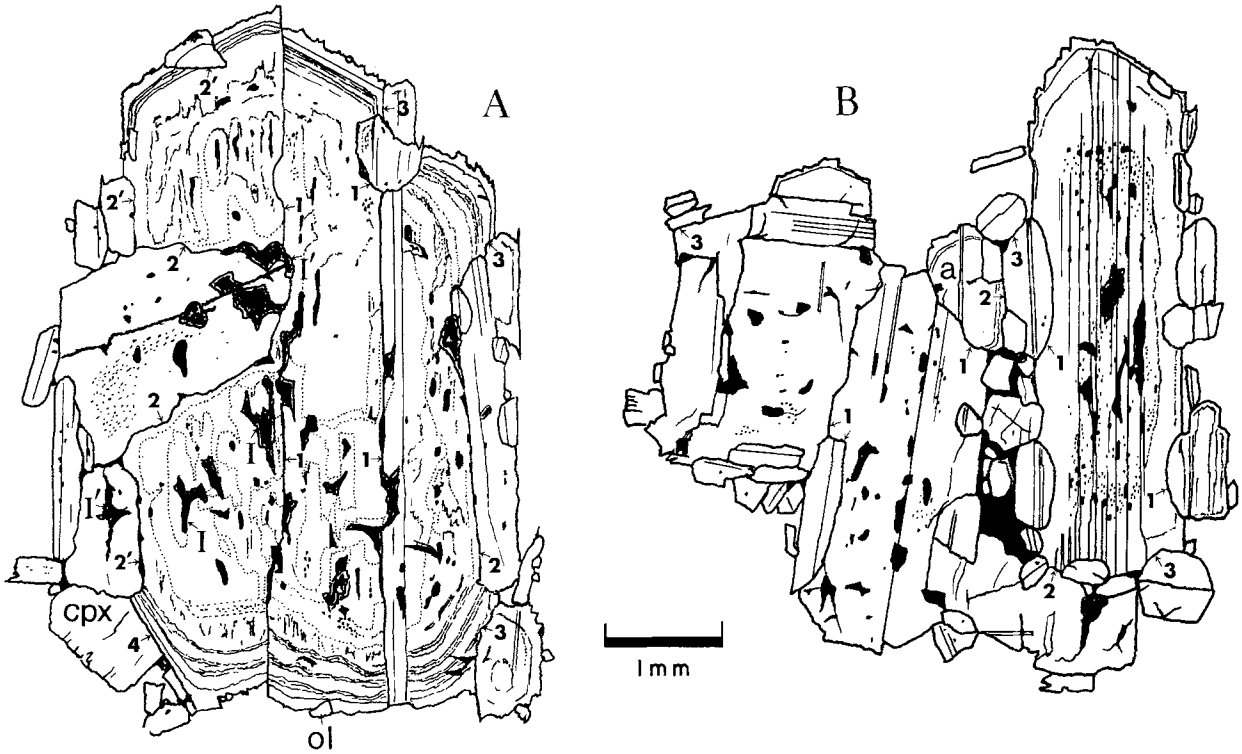

Fig. 8A, B. Sketches of plagioclase glomerocrysts showing complex mode of attachment among single grains. **A** A glomerocrysts from 395A-17-1,106-112A. Skeletal plagioclase grains attached together along boundaries labeled 1 during early stage of crystallization. The boundaries labeled 2 and 2′ represent the second stage of attachment (2′ was a little later than 2). The third stage of attachment along the boundaries labeled 3 occurred during the development of the high-An zone in the outer part of the mantle. An olivine, a clinopyroxene, and several plagioclase grains attached to the inner rim of the host glomerocryst during the last stage of attachment. Inclusions such as I developed from the skeletal growth of the core, whereas those like I′ are melt enclosed during attachment. **B** A glomerocryst from 395A-23-1,98-103 that is composed of plagioclase grains joined along boundary 1 (*left and lower part*) and a large, polysynthetically twinned plagioclase with a skeletal core (*right part*). These two parts attached along boundaries 2 and enclosed one olivine, two spinel, and several plagioclase grains with basaltic liquid. The last stage attachment is marked by 3. See text for discussion

that Fe content in plagioclase shows a similar but stronger trend. It follows that the Mg/(Mg+Fe) ratio in plagioclase should decrease slightly with decreasing temperature. Combination of the equations for the temperature dependence of the distribution coefficients for Mg and Fe in plagioclase-basalt system (Longhi 1976) and the equilibrium temperature-composition relationship in the system albite-anorthite yields a straight line with the slope of 0.0042 for the relationship between bulk composition and Mg/(Mg+Fe) value in plagioclase at equilibrium (Fig. 5, solid line).

Kinetic Effects

Under equilibrium conditions a silicate melt crystallizes when it reaches its liquidus temperature. In natural systems, however, magma cools at a finite rate and to get a finite rate of crystallization the liquid must be supercooled a finite amount. The relationships between the degree of supercooling, composition, growth rate, and crystal morphology have been studied for phases occuring in basalts by several investigators including Lofgren (1972, 1974), Donaldson (1976), Coish and Taylor (1979), Kirkpatrick (1979b), and Kirkpatrick et al. (1979). Lofgren (1972) showed that the composition of the plagioclase growing from a supercooled liquid at about 6 kb water pressure is significantly more albitic and the liquid significantly more anorthitic than at equilibrium. For experiments in which the sample is rapidly cooled to some undercooling and then held at a constant temperature the experimental charge approaches equilibrium and the crystals are reversely zoned (Smith and Lofgren 1979).

Under isothermal conditions, the initial deviation from the equilibrium crystal composition increases with increasing supercooling and can be determined from the compositional difference between the core and its surrounding, reverse zoned rim. Therefore, it is possible to calculate the kinetic effect on the Mg and Fe contents in the skeletal plagioclase cores (e.g., Fig. 4A, B, G) by using a crystal composition of 78% An instead of 75% An. The slope of the Mg/(Mg+Fe) ratio versus % An plot is 0.0042, which is the same as for the equilibrium condition. This is due to the very gentle curvature of the solidus in this composition range.

The variation of crystal morphology with supercooling in the anorthite-albite system at the water pressure of about 6 kb was examined by Lofgren (1974). Plagioclase crystallizes with a tabular morphology at low undercoolings. The same morphologic variation with supercooling has been observed by Kirkpatrick et al. (1979) for dry 1 atm experiments with synthetic albite-anorthite compositions. In these experiments plagioclase morphology varies from euhedral to skeletal/dendritic to spherulitic within a supercooling range of 75° C. It seems likely, then, that skeletal zones in the Legs 45 and 46 plagioclase phenocrysts crystallized at larger undercoolings than zones with euhedral morphologies.

Kirkpatrick et al. (1979) investigated the growth rate of plagioclase from synthetic plagioclase liquids as a function of supercooling and composition. They found that the growth rate increases with increasing anorthite content and that the supercoolings with the maximum growth rates are about 150° C. Except

for very albitic plagioclase, the growth rates increase rapidly to the maximum and then gently decrease with increasing supercooling. For a bulk composition of $An_{75}Ab_{25}$ the growth rate increases about 100 times for a change in supercooling from 20 to 70° C.

Therefore, crystals suspended in a suddenly supercooled melt will grow more rapidly and with the new crystal being more albitic. The new crystal is also likely to contain abundant glass inclusions due to the much faster growth and high supersaturation (Tiller 1977). This feature was observed by Watson (1976) in plagioclase crystals from a tholeiitic basalt dredged near Bouvet Island in which glass inclusions are concentrated in several bands with more albitic composition than the surrounding material.

Magma Mixing

Mixing of the chemically distinctive magmas is a widespread petrological process and has been applied frequently to interpret the origin of many acidic and intermediate volcanic rocks (see Anderson 1976, for a review). Recent investigations of MORBs have shown that magma mixing probably plays a significant role in their formation also (e.g., Dungan and Rhodes 1978, 1980; Rhodes et al. 1979a, b; Walker et al. 1979). In particular, Walker et al. (1979), by plotting analyses of about 2,000 MORBs onto a plagioclase saturated diopside-olivine-silica phase diagram, demonstrated that MORB compositions cluster along the ol-plag-high Ca cpx cotectic. They attribute the extreme scarcity of low-Ca cpx saturated MORB, which should be a common composition if differentiation were a dominant process, to the repeated mixing of primitive and more evolved magmas such that the hybrid rarely reaches low-Ca cpx saturation.

The variation of plagioclase compositions and morphologies due to the mixing of two chemically distinctive magmas can be illustrated by a simplified model in the albite-anorthite system (Fig. 9). Suppose that liquids L1 at T1 and L2 at T2 are mixed in the proportions to give a hybrid liquid, L3. L3 will be at T3 provided that the enthalpy of mixing is small and the heat capacities of the liquids are identical. Crystals in equilibrium with L2 would be superheated to X2′ and therefore be resorbed or even completely dissolved; whereas crystals in equilibrium with L1 would be supercooled to X1′. Crystals of composition X3 start to grow from L3, and continued growth produces reverse zoned crystals until a new equilibrium is reached, as represented by L4–X4 pair. This process will result in two kinds of zoning patterns: a euhedral or slightly resorbed core of higher An content surrounded by a skeletal, more albitic, reversed zone; and a resorbed core of lower An content followed by a more anorthitic, reversed zone. The actual zoning and morphologic variations across the boundary depend on the relative amount of the magmas actually mixed, their compositions, and the thermal condition in the magma chamber. For instance, if the hybrid continues to cool and differentiate immediately after mixing, the temperature at which X3 begins to crystallize will be lower than T3 and the reverse zoning X3–X4 might shrink or disappear and be replaced by normal zoning. If the temperatures and compositions of the mixed liquids are so close that the supercooling of X1 is not large, then X1′ would be surrounded by a non-skeletal zone of growth. The compositional differences between X2′–X3 and X1′–X3 decrease with a decreasing difference between the magma compositions. Because of the very gentle curvature of the liquidus surface the supercooling of the liquid during mixing would appear to be small, therefore L3 cannot be far from equilibrium and the zone X3–X4 must be narrow.

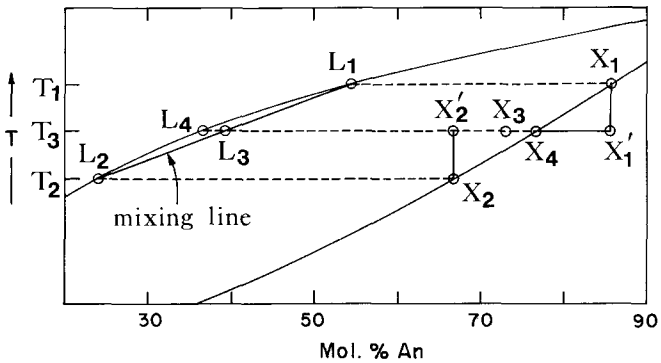

Fig. 9. Part of the system albite-anorthite showing the equilibrium relationships between crystal and liquid during mixing under isothermal condition. See text for discussion

The major effects of this kind of binary magma mixing are superheating with respect to the low-An plagioclases and supercooling with respect to the high-An plagioclases and, in both cases, an abrupt change of composition of the plagioclase crystallizing. In addition, mixing of two liquids, in this case L1 and L2, will limit the resulting plagioclase composition roughly between their equilibrium compositions, X1 and X2. It follows that repeated, binary mixing with a limited composition range leads to the alternating high-An and low-An zones, but no 'ladder' shaped zoning patterns can be produced.

During mixing the addition of plagioclase crystals, in this case more anorthitic glomerocrysts and megacrysts, to the more evolved liquid will reduce the extent of differentiated liquid and therefore minimize the range of An content of cotectic plagioclase (McBirney 1979). This is manifested by our observation that the composition range of the base lines in the mantle is smaller than that between ol-plag cosaturation and ol-plag-cpx cosaturation (Dungan et al. 1979b).

Dynamic Effects

Magma stored in a chamber of finite size tends to convect in response to the temperature difference between upper and lower boundaries of the chamber. As described by Maaløe (1976), convection of magma in the chamber starts with many small, local turbulent currents and ends up with most of the magma body involved in large scale flow. The properties of the large scale flow regime are controlled by the Rayleigh number, R, which is given by

$$R=\alpha \Delta T d^3 g/\nu\kappa,$$

where α is the thermal expansion coefficient, d the thickness of the fluid layer, ΔT the temperature difference between the top and bottom of the layer, g the acceleration due to gravity, ν the kinematic viscosity ($\nu=\eta/\rho$, where η is the shear viscosity and ρ is the density), and κ the thermal diffusivity. For a layer of fluid held between two plates at constant temperature convection will occur if R is greater than about 1,700, and the convection will be turbulent if R is greater than about 5×10^8 (Landau and Lifshitz 1959). For typical MORB compositions $\alpha=6.9\times10^{-5}$° C^{-1}, $\rho=2.7$ gm cm^{-3} (Bottinga and Weill 1970; Nelson and Carmichael 1979), $\eta=4\times10^2$ gm cm^{-1} sec^{-1} (Bottinga and Weill 1972), and $\kappa=1\times10^{-2}$ cm^2 sec^{-1}. Thus for a 10° C temperature difference between the top and bottom of the chamber, the convection will be turbulent for a chamber larger than 15 m thick. For a 1 km thick body the convection will be turbulent if ΔT is greater than about 4×10^{-5}° C. It

appears, therefore, that free convection in sub-ridge magma chambers should be turbulent. In addition, since the heat loss through the upper wall, assuming the temperature in the country rock increases with increasing depth, is always greater than through the floor, a temperature gradient in the chamber exists even if convection occurs. Therefore, turbulent convection in the chamber is maintained once it starts. The rate of material transfer is enhanced by this turbulent convection and efficient mixing is likely to occur.

Convection in a chamber, however, can be interrupted when a pulse of hotter magma is injected into it. During a transient period, the new, hotter magma may be less dense than the magma already in the chamber and will tend to rise to the top (Sparks et al. 1980). The temperature gradient in the chamber is then eliminated, and turbulent convection ceases. Moreover, partial mixing of the new magma and the differentiating magma already in the chamber is likely to occur during the upward movement of the hotter magma (Sparks and Sigurdsson 1977). Small scale convection in the chamber will start again when this newly mixed magma cools sufficiently, and the partially mixed magma and the remaining old, more evolved magma will begin to mix. It is during this turbulent convection stage that synneusis is likely to occur (Vance 1969). After this, large scale turbulent flow will be reestablished and the magma will be gradually fully mixed.

Petrologic Processes Under the Mid-Atlantic Ridge

Based on the models of a sub-ridge steady-state magma chamber developed by, for example, Bryan and Moore (1977), O'Hara (1977), Dungan and Rhodes (1978), and on its dynamic behavior discussed above, it is possible to postulate the following cycle of events in a magma chamber beneath the mid-Atlantic ridge: (1) injection of primitive magma from the mantle into a homogeneous, relatively fractionated, turbulently convecting magma chamber below the ridge, (2) rise of this hotter, less dense, primitive magma through the chamber to its top, partial mixing of this magma with some of the evolved magma, and suppression of convection in the chamber by the hotter magma on the top, (3) intrusion of part of this partially mixed magma into the sheeted dike system, (4) cessation of intrusion and cooling of the remaining partially mixed magma, (5) establishment of small scale turbulent convection which begins to mix the partially mixed and the evolved magmas, and (6) gradual development of large scale turbulent convection which homogenizes these two magmas and returns the magma to approximately its state before stage (1).

Stages 1 and 2: Core-Forming Stages

We suggest that the cores of the plagioclase phenocrysts formed during stages 1 and 2. The compositions of the cores are too anorthitic to have crystallized from an evolved melt (Rhodes et al. 1979b), so they could not have formed during any of the later stages. It is also unlikely that they crystallized from a primitive magma at high pressures in the upper mantle prior to injection into the magma chamber, because they would be more albitic, and the pressure decrease during injection would cause dissolution. It is possible, however, that the rare resorbed albitic inner cores that are not skeletal could have crystallized at high pressures.

Assuming that most of the cores formed during stages 1 and 2, the morphological and compositional variations can be interpreted in the following way. During injection and mixing the primitive magma was undercooled in two ways – by cooling in contact with the evolved magma and by mixing with it. Thus, during stages 1 and 2 there were volumes of primitive and partially mixed magma at a variety of undercoolings. The euhedral, tabular, high-An cores grew at relatively small undercoolings in melt composed of mostly primitive magma. The skeletal, low-An cores grew at larger undercoolings from melt containing a larger percentage of evolved magmas and then continued to grow at reduced undercooling as the partial mixing became more thorough. The consistent correlation between Mg/(Mg+Fe) and An content in the cores (Fig. 5) indicates that all the cores formed from similar primitive magma regardless of the subsequent history of magma evolution which produced the distinctive compositions of the individual chemical units.

Stages 5 and 6: Mantle-Forming Stages

Because of their complex patterns of compositional zoning and inclusion entrapment, the mantles of the complexly zoned plagioclase must have developed during a period of changing melt composition and undercooling. It seems most likely that this happened during the reestablishment of convection in the chamber (stages 5 and 6 of the cycle). During the incipient stage of convection where small scale turbulent flow was dominant (stage 5), the chemical differences between the partially mixed and the evolved magmas were large enough that local mixing of the two magmas or transfer of crystals from one magma to another gave rise to the spikes/plateaus. In the regions where mixing was occurring, plagioclases with relatively albitic compositions at their rims which were suddenly exposed to the partially mixed, less evolved magma were resorbed and then overgrown by a more anorthitic layer. Relatively anorthitic plagioclases rapidly exposed to the more evolved magma might have been slightly resorbed at first but were then rapidly overgrown by a more albitic layer, with or without formation of inclusions. The crystals with a skeletal morphology in the mantle very close to the core-mantle boundary grew in regions of large undercooling in the chamber during reestablishment of convection.

After the local mixing was completed, crystals started to grow in the locally mixed magma to form the segments of the base line in the zoning profile. Progressive homogenization of the magma due to repeated mixing resulted in alternating spikes/plateaus and base line in the mantle region and a decrease in the compositional difference between magmas so that the spikes and plateaus became fewer and smaller. After turbulent convection became operative over the entire chamber (stage 6), the mixed magma reached uniform composition and continued to differentiate, resulting in growth of plagioclase with a more albitic composition but without any spikes or plateaus.

Stages 1 and 2 of the Next Cycle: Outermost Mantle-Forming Stages

The ubiquitous high-An plateau at the outside of the mantle is most likely due to the incorporation of the plagioclases growing during stage 6 into the next pulse of injected primitive magma at stage 1 of the cycle. Again there was partial mixing between this new pulse of magma and the evolved one. At this time a part of the albitic mantle of the plagioclases was resorbed and the remaining crystal overgrown by a plateau of uniform, more anorthitic composition. The time span between mixing of magmas and intrusion of this hybrid might be so small that only some plagioclase crystals have a growth from the hybrid,

as indicated by the less anorthitic outer part of the plateau (Fig. 4A–C).

The abrupt temperature increase in the chamber due to the injection of hot, primitive magma again disrupted the turbulent convection within the chamber, allowing plagioclase crystals to float to the top of the chamber and causing extensive synneusis. The infrequent occurrence of simply zoned plagioclases in these basalts is, perhaps, due to their higher density, which prevents them from floating to the top and being incorporated in the magma intruded into the sheeted dikes (Campbell et al. 1978).

Because of the cyclic nature of the processes, both cores and the outermost mantles were crystallizing during stages 1 and 2. The comparable compositions in the high-An cores and outermost mantles probably indicate chemical similarity among each pulse of primitive magma injected.

Stage 3: Inner Rim-Forming Stage

The drastic decrease in An content along with the occurrence of oscillatory zoning in the inner rim requires efficient heat loss from the host magma (Pringle et al. 1974). The most reasonable interpretation for this is that the inner rim formed during the intrusion of part of the partially mixed, plagioclase-bearing magma into the sheeted dike system between the chamber and the ocean floor. It can also be inferred from the mostly euhedral mantle-rim boundaries that the inner rim crystallized under disequilibrium conditions due to the rapid removal of heat from the magma (see Vance 1965, p. 646). The different zoning sequences in the inner rims from grain to grain probably reflect differing local thermal conditions in the sheeted dike system.

The consistent correlation between Mg/(Mg+Fe) values in plagioclase and in host rock from distinct chemical units (Fig. 6) suggests that the chemical characteristics of each batch of mixed magma were established at or before growth of the inner rim and intrusion into the sheeted dike system. We propose that magmatic differentiation is the major process operating at this time. If this is the case, and we assume that the composition of the mixed magma at both sites is very close, as indicated by the melt inclusion data (Dungan and Rhodes 1978), then the width of inner rim should correlate with the time span the magma remained in the sheeted dikes and therefore to the amount of differentiation taking place in this time interval. This agrees with the relatively thicker inner rims of the generally more evolved Site 395 basalts and the relatively thinner inner rims in the generally less evolved Site 396 basalts (Dungan and Rhodes 1978).

During this stage, the large plagioclase crystals tend to rotate to the middle of these conduits (Bhattacharji and Smith 1964) so that synneusis between large crystals along their broader surfaces is less likely than that between large and smaller crystals. The residence time of the magma in the sheeted dikes must be relatively short because the inner rim is narrow. It is suggested then that the injection of primitive magma along with magma mixing is the major mechanism for triggering the eruption of the phyric basalts (see also Sparks and Sigurdsson 1977; Sparks et al. 1980).

Conclusions

The complex zoning patterns of plagioclase phenocrysts in mid-Atlantic ridge basalts can be explained by a model involving mixing of evolved and primitive magma in a sub-ridge magma chamber.

There are two important implications in the present model. (1) Kinetic effects play a vital part in controlling the course of magmatic evolution, during both mixing and crystallization, as reflected by the disequilibrium textures (Dungan et al. 1979a) and complex chemical/morphological variations in plagioclase crystals in these phyric basalts. (2) The fluid dynamic calculations indicate that the processes suggested could occur even in magma chambers which are too small (e.g., 1–2 km high) to be detected by seismic refraction methods. Therefore the discrepancy between petrologic and seismic modelling of mid-Atlantic ridge at the FAMOUS area proposed by Bryan and Moore (1977) and Fowler (1978) can be reconciled, and it appears that it is unnecessary to assume a large magma chamber to account for the origin of these basalts.

Acknowledgments. We thank Professor Albert T. Hsui for profitable discussions of the fluid dynamic aspects of magma bodies. Professors Donald M. Henderson and David E. Anderson reviewed an early draft. The paper has also benefited from the critical reviews of Drs. Wilfred B. Bryan, Bernard W. Evans and an anonymous referee. The samples studied were provided by the Deep Sea Drilling Project at San Diego, California. Mrs. Carol Sanderson is acknowledged for her competent help with the manuscript. This study was supported by NSF grants EAR-7682185 and EAR-7903923.

References

Anderson AT (1976) Magma mixing: petrological process and volcanological tool. J Volcanol Geotherm Res 1:3–33

Bhattacharji S, Smith CH (1964) Flowage differentiation. Science 145:150–153

Blanchard DP, Rhodes JM, Dungan MA, Rodgers KV, Donaldson CH, Brannon JC, Jacobs JW, Gibson EK (1976) The chemistry and petrology of basalts from Leg 37 of the Deep Sea Drilling Project. J Geophys Res 81:4231–4246

Bottinga Y, Weill DF (1970) Densities of liquid silicate systems calculated from partial molar volumes of oxide components. Am J Sci 269:169–182

Bottinga Y, Weill DF (1972) The viscosity of magmatic silicate liquids: a model for calculation. Am J Sci 269:169–182

Boyd FR, Finger LW, Chayes F (1969) Computer reduction of electron-probe data. Carnegie Inst Washington Yearb 67:210–215

Bryan WB, Moore JG (1977) Compositional variation of young basalts in the mid-Atlantic ridge rift valley near 36°49′N. Bull Geol Soc Am 88:556–570

Campbell IH, Roeder PL, Dixon JM (1978) Plagioclase buoyancy in basaltic liquids as determined with a centrifuge furnace. Contrib Mineral Petrol 67:369–377

Coish RA, Taylor LA (1979) The effects of cooling rate on texture and pyroxene chemistry in DSDP Leg 34 basalt: a microprobe study. Earth Planet Sci Lett 42:389–398

Delaney JR, Muenow D, Ganguly J, Royce D (1977) Anhydrous glass-vapor inclusions from phenocrysts in oceanic tholeiitic pillow basalts. EOS 58:530

Dewey JF, Kidd WS (1977) Geometry of plate accretion. Bull Geol Soc Am 88:960–968

Donaldson CH (1976) An experimental investigation of olivine morphology. Contrib Mineral Petrol 57:187–213

Dungan MA, Rhodes JM (1978) Residual glass and melt inclusions in basalts from DSDP Legs 45 and 46: evidence for magma mixing. Contrib Mineral Petrol 67:417–431

Dungan MA, Rhodes JM (1980) Magma mixing at mid-ocean ridges. EOS 61:67

Dungan MA, Rhodes JM, Long PE, Blanchard DP, Brannon JC, Rodgers KV (1979a) The petrology and geochemistry of basalts from Site 396, Legs 45 and 46 of the Deep Sea Drilling Project. Initial Reports of the Deep Sea Drilling Project 46:89–113

Dungan MA, Long PE, Rhodes JM (1979b) The petrology, mineral chemistry, and one-atmosphere phase relations of basalts from Site 395. Initial Reports of the Deep Sea Drilling Project 45:461–477

Engel AEJ, Engel CG, Havens RG (1965) Chemical characteristics of oceanic basalts and the upper mantle. Bull Geol Soc Am 76:719–734

Flower MFJ, Ohnmacht W, Schmincke HU, Gibson IL, Robinson PT, Parker R (1979) Petrology and geochemistry of basalts from Hole 396B, Leg 46. Initial Reports of the Deep Sea Drilling Project 46:179–213

Fowler CMR (1978) The mid-Atlantic ridge: structure at 45°N. Geophys J R Astron Soc 54:167–183

Frey FA, Bryan WB, Thompson G (1974) Atlantic Ocean floor: geochemistry and petrology of basalts from Legs 2 and 3 of the Deep Sea Drilling Project. J Geophys Res 79:5507–5527

Green TH (1967) High pressure experimental investigations on the origin of high-alumina basalt, andesite, and anorthosite. PhD Dissertation, Australian National Univ, Canberra, Australia

Greenbaum D (1972) Magmatic processes at ocean ridges: evidence from the Troodos Massif, Cyprus. Nature (Phys Sci) 238:18–21

Imsland P, Larsen JG, Prestvik T, Sigmond EM (1977) The geology and petrology of Bouvetoya, South Atlantic Ocean. Lithos 10:213–234

Irvine TN (1979) Rocks whose composition is determined by crystal accumulation and sorting. In: HS Yoder, Jr (ed) The evolution of the igneous rocks. Princeton University Press, Princeton, New Jersey, pp 245–306

Jackson ED, Green II HW, Moores EM (1975) The Vourinos Ophiolite, Greece: cyclic units of lineated cumulates overlying harzburgite tectonite. Bull Geol Soc Am 86:390–398

Kay RW, Hubbard NJ, Gast PW (1970) Chemical characteristics and origin of oceanic ridge volcanic rocks. J Geophys Res 75:1585–1613

Kirkpatrick RJ (1979a) Petrology of basalts: Hole 396B, DSDP Leg 46. Initial Reports of the Deep Sea Drilling Project 46:165–178

Kirkpatrick RJ (1979b) Processes of crystallization in pillow basalts, Hole 396B, DSDP Leg 46. Initial Reports of the Deep Sea Drilling Project 46:271–282

Kirkpatrick RJ, Klein L, Uhlmann DR, Hays JF (1979) Rates and processes of crystal growth in the system anorthite-albite. J Geophys Res 84:3671–3676

Landau LD, Lifshitz EM (1959) Fluid Mechanics. Pergamon, England

Lindsley DH (1966) Melting relations of plagioclase at high pressures. Carnegie Inst Washington Yearb 65:204

Lofgren G (1972) Temperature induced zoning in synthetic plagioclase feldspar. In: WS MacKenzie, J Zussman (eds) The Feldspars. Manchester University Press, Manchester, England, pp 362–375

Lofgren G (1974) An experimental study of plagioclase crystal morphology: isothermal crystallization. Am J Sci 274:243–273

Longhi J (1976) Iron, magnesium and silica in plagioclase. PhD Thesis, Harvard University, Cambridge, Massachusetts

Maaløe S (1976) The zoned plagioclase of the Skaergaard intrusion, East Greenland. J Petrol 17:398–419

McBirney AR (1979) Effects of assimilation. In: HS Yoder JR (ed) The Evolution of the Igneous Rocks. Princeton University Press, Princeton, New Jersey

Melson WG, Vallier TL, Wright TL, Byerly G, Nelson J (1976) Chemical diversity of abyssal volcanic glass erupted along Pacific, Atlantic and Indian Ocean sea-floor spreading centers. In: GH Sutton, MH Manghani, R Moberly (eds) The geophysics of the Pacific Ocean Basin and its margin. AGU Geophys, Monography 19 (The Wollard Volume)

Muir ID, Tilley CE (1964) Basalts from the northern part of the rift zone of the mid-Atlantic ridge. J Petrol 5:409–434

Natland JH (1979) Crystal morphologies in basalts from DSDP Site 395, 23°N, 46°W, mid-Atlantic ridge. Initial reports of the Deep Sea Drilling Project 46:423–445

Nelson SA, Carmichael ISE (1979) Partial volumes of oxide components in silicate liquids. Contrib Mineral Petrol 71:117–124

O'Hara MJ (1977) Geochemical evolution during fractional crystallization of a periodically refilled magma chamber. Nature 266:503–507

Pallister JS, Hopson CA (1981) Semail ophiolite plutonic suite: field relations, phase variation, cryptic variation and layering, and a model of a spreading ridge magma chamber. J Geophys Res 86:2593–2644

Pankhurst RJ (1977) Open system crystal fractionation and incompatible element variation in basalts. Nature 268:36–38

Pringle GJ, Trembath LT, Parjari Jr GE (1974) Crystallization history of a zoned plagioclase. Mineral Mag 39:867–877

Rhodes JM, Blanchard DP, Rodgers KV, Jacobs JW, Brannon JC (1976) Petrology and geochemistry of basalts from the Nazca plate: part 2 – major and trace element chemistry. Initial Reports of the Deep Sea Drilling Project 34:239–244

Rhodes JM, Blanchard DP, Dungan MA, Rodgers KV, Brannon JC (1979a) Chemistry of Leg 45 basalts. Initial Reports of the Deep Sea Drilling Project 45:447–459

Rhodes JM, Dungan MA, Blanchard DP, Long PE (1979b) Magma mixing at mid-ocean ridges: evidence from basalts drilled near 22°N on the mid-Atlantic ridge. Tectonophysics 55:35–61

Shibata T, DeLong SE, Walker D (1979) Abyssal tholeiites from the oceanographer fracture zone I. Petrology and fractionation. Contrib Mineral Petrol 70:89–102

Smewing JD (1979) Mixing characteristics and compositional differences in mantle-derived melts beneath spreading axes: evidence from cyclic units in the ophiolite of North Oman. EOS 60:962

Smith JV (1975) Some chemical properties of feldspars. In: PH Ribbe (ed) Feldspar Mineralogy. Mineral Soc Am Short Course Notes, Vol 2, Chap 9

Smith RK, Lofgren FE (1979) The physico-chemical and crystal growth kinetics necessary for zonal development in plagioclase. Geol Soc Am Abstr Progr 7:520

Sparks RSJ, Sigurdsson H (1977) Magma mixing: a mechanism for triggering acid explosive eruptions. Nature 267:315–318

Sparks RSJ, Meyer P, Sigurdsson H (1980) Density variation amongst mid-ocean ridge basalts: implications for magma mixing and the scarcity of primitive lavas. Earth Planet Sci Lett 46:419–430

Stern C (1979) Open and closed system igneous fractionation within two Chilean ophiolites and the tectonic implication. Contrib Mineral Petrol 6:243–258

Stewart DB, Walker GW, Wright TL, Fahey JJ (1966) Physical properties of calcic labradorite from Lake County, Oregon. Am Mineral 51:177–197

Subbarao KV, Ferguson RB, Turnock AC (1972) Zoned plagioclase from Elbow Lake, Manitoba 1. Comparative microprobe and optical analysis. Can Min 11:488–503

Sun SS, Nesbitt RW, Sharaskin AYa (1979) Geochemical characteristics of mid-ocean ridge basalts. Earth Planet Sci Lett 44:119–138

Tiller WA (1977) On the cross-pollenation of crystallization ideas between metallurgy and geology. Phys Chem Minerals 2:125–151

Uebel PJ (1978) The zoning of plagioclase as record of petrogenetic development of the Ben Nevis Ring-Intrusion, Scotland. Neues Jahrb Mineral Abh 132:182–213

Vance JA (1965) Zoning in igneous plagioclase: patchy zoning. J Geol 73:636–651

Vance JA (1969) On synneusis. Contrib Mineral Petrol 24:7–29

Walker D, Shibata T, DeLong SE (1979) Abyssal tholeiites from the oceanographer fracture zone II. Phase equilibria and mixing. Contrib Mineral Petrol 70:111–125

Watson EB (1976) Glass inclusions as samples of early magmatic liquid: determinative method and application to a south Atlantic basalt. J Volcanol Geotherm Res 1:73–84

White WM, Schilling JG (1978) The nature and origin of geochemical variation in mid-Atlantic ridge basalts from the central north Atlantic. Geochim Cosmochim Acta 42:1501–1516

Wiebe RA (1968) Plagioclase stratigraphy: a record of magma conditions and events in a granitic stock. Am J Sci 266:690–703

Yoder Jr HS (1969) Experimental studies bearing on the origin of anorthosite. In: YW Isachsen (ed) Origin of anorthosite and related rocks. New York State Mus Sci Serv Mem 18, pp 13–22

Received June 9, 1981; Accepted in revised form January 18, 1982